Fluid 'rope trick' investigated

Buckling instabilities can arise from competition between axial compression and bending in slender objects. These are not restricted to solids, but also occur with fluids with free surfaces[1–4], in geophysics[5] and in materials processing[6]. Here we consider a classic demonstration of fluid buckling[7].

When honey is poured from a sufficient height, it approaches one's toast as a thin filament which whirls steadily around the vertical forming a regular helical coil (illustrated with silicone oil in Fig. 1), a behaviour reminiscent of the coiling of a falling flexible rope[8]. We derive a scaling law that predicts the coiling frequency in terms of the filament radius and the flow rate.

The physical parameters governing the phenomenon include the fluid density ρ, viscosity μ (kinematic viscosity $\nu = \mu/\rho$), the flow rate Q, gravity g, a characteristic filament radius r, and the height, h, over which the filament falls. As h is gradually increased, the axial stagnation flow becomes unstable to bending disturbances and the filament is steadily laid out in a circular coil of radius R at a frequency Ω.

The onset of the instability[9–11] is determined by the relative magnitude of the gravitational timescale $(h/g)^{1/2}$ and the viscous timescale $r^2\rho/\mu$, characterized by a slenderness ratio $\epsilon = r/h$, or a Reynolds number $\mathrm{Re} = gr^3/\nu^2$. We note that a similar parameter $\rho g h^3/B$, where B is the bending stiffness, occurs in the elastic analogue[8]. Only below a critical value of ϵ or Re is the axisymmetric stagnation flow unstable. Far from onset, when ϵ becomes sufficiently small, the flow is still mainly an axial stretching flow. However, in a small neighbourhood of the flat surface there is a highly nonlinear coiling region, which persists over a range of falling heights.

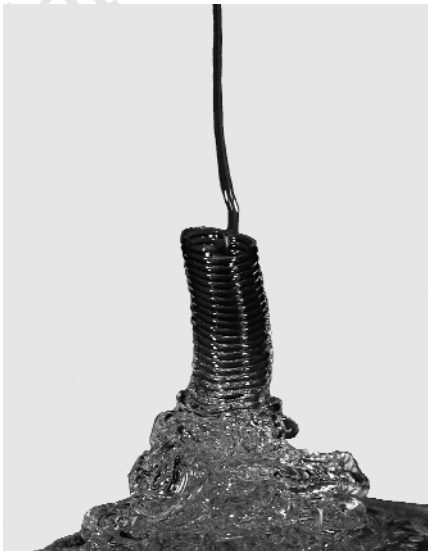

FELICE FRANKEL

Figure 1 Photograph of a coiling filament of silicone oil (PDMS, μ=1.019 × 10^3 g cm^{-1} s, ρ=1 g cm^{-3}; Gelest), highlighting the constant-diameter coils of diameter of approximately 0.5 cm near the surface.

In this region, the filament radius is constant (Fig. 1), and the rotatory inertial forces due to the whirling dominate gravity and are balanced by the viscous forces due to the differential velocities between the inner and outer segments of a curved filament. The characteristic radius of curvature of the filament scales with the coil radius R, as for a coiling rope[8]. Then the differential velocity scales as Ur/R, where U is the axial velocity. The Newtonian viscous force per unit volume scales as $\mu Ur/R^3$. The force per unit volume due to centripetal and Coriolis accelerations scales as $\rho\Omega^2 R$. Balancing the two forces yields

$$\mu Ur/R^3 \sim \rho\Omega^2 R \qquad (1).$$

A filament of almost constant diameter is laid out in a steady circular coil near the flat surface $U \sim \Omega R$, whereas continuity of the axial stretching flow yields $Ur^2 \sim Q$. Substituting these relations into equation (1) yields a scaling law for the coiling frequency

$$\Omega \sim Q^{3/2} r^{-7/2} \nu^{-1/2} \qquad (2).$$

To test these predictions, we studied the coiling of silicone oil, flowing at a constant rate out of circular holes in a steel plate at the base of a large reservoir of fluid. We established the dependence between the coiling frequency and filament radius by varying the height of the fall. The coiling frequency was determined by measuring the intensity fluctuations of a refracted laser aimed at the top of the coiling region. A horizontal microscope with a charge-coupled device camera was used to measure the filament radius with an accuracy of 1%. All measurements were made in a parameter regime far from the onset of coiling and also far from the regime when the coiled column itself is unstable and collapses periodically under its own weight. The data are best fitted by a power law $\Omega/Q^{1.5} \sim r^{-3.58\pm.16}$ for each flow rate (Fig. 2), and agree well with the theoretically predicted scaling law(2).

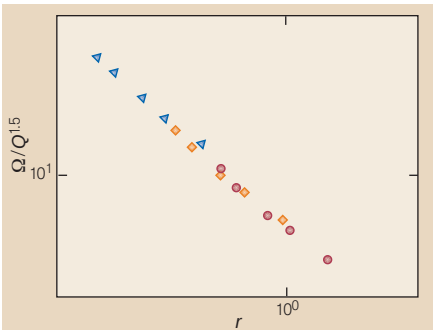

Figure 2 Log–log plot of the normalized coiling frequency (Ω/Q^{15}) against filament radius (r). Triangle: hole radius, 3.2 mm, Q=0.56 g s^{-1}; diamond: hole radius, 4.0 mm, Q =0.96 g s^{-1}; circle: hole radius, 4.8 mm, Q=1.28 g s^{-1}. The data are fitted by the relation $\Omega/Q^{15} \sim r^{3.58}$ for each flow rate, and confirm equation (2).

Several effects such as surface tension, the relaxation of Poiseuille flow to plug flow in the neighbourhood of the orifice, air drag, non-Newtonian effects and the effect of gravity in the coiling region, have been neglected here, as they are relatively unimportant. They can be accounted for in a quantitative long-wavelength theory similar to that used to describe coiling of falling ropes[8].

L. Mahadevan
Division of Mechanics and Materials, Mechanical Engineering,1-310, Massachusetts Institute of Technology, Cambridge, MA 02139, USA
e-mail: l_m@mit.edu
William S. Ryu, Aravinthan D.T. Samuel
Department of Molecular and Cellular Biology, Harvard University, Cambridge, MA 02138, USA and Rowland Institute of Science, Cambridge, MA 02142, USA

1. Barnes, G. & Woodcock, R. *Am. J. Phys.* 26, 205–209 (1958).
2. Taylor, G. I. *Proc. 12th Intl Congr. Appl. Mech.* 382–395 (1969).
3. Benjamin, T. B. & Mullins, T. J. *Fluid Mech.* 195, 523–540 (1988).
4. Matovich, M. A. & Pearson, J. R. A. *Ind. Engrg. Chem. Fund.* 8, 605–609 (1969).
5. Johnson, A. M. & Fletcher, R. C. *Folding of Viscous Layers* (Columbia University Press, New York, 1994).
6. Rawson, H. *Phys. Tech.* 2, 91–114 (1974).
7. Taylor, G.I. *Low Reynolds Number Flows* (*Encyclopaedia Britannica* films, 1967).
8. Mahadevan, L. & Keller, J. B. *Proc. R. Soc. Lond. A* 452, 1679–1694 (1996).
9. Cruickshank, J. O. & Munson, B. R. *J. Fluid Mech.* 113, 221–239 (1981).
10. Griffiths R. W. & Turner, J. S. *Geophys. J.* 95, 397–419 (1988).
11. Tchavdarov, B., Yarin, A. L. & Radev, S. *J. Fluid Mech.* 253, 593–615 (1993).

Alzheimer's peptide kills cells of retina *in vivo*

Alzheimer's disease, the commonest form of dementia, is a progressive, age-dependent disorder characterized by the presence of large numbers of senile plaques and neurofibrillary tangles[1]. The neuritic plaques consist of an accumulation of amyloid-β peptide (Aβ); this substance, which derives from proteolysis of β-amyloid precursor protein (APP), seems to play a central role in the pathology of the disease. The toxicity of Aβ to neurons has already been demonstrated *in vitro*. Here we show that the peptide is also cytotoxic *in vivo*.

Support for the role of Aβ in Alzheimer's comes from reports showing that mutations in the gene encoding APP, and in other genes involved in the disease, lead to overproduction of the more amyloidogenic 42 amino-acid residue long isoform of Aβ, $Aβ_{1–42}$. Transgenic mice overexpressing the gene for APP show similar changes, and aggregated Aβ is toxic to cultured neurons of the cerebral cortex or

paternal pronuclei analysed after 8 hours showed very little methylation (Fig. 1c).

To prevent DNA replication, one-cell embryos were collected after 6 hours and cultured for a further 10 hours in the presence of aphidicolin (at 2 μg ml^{-1})[6]. The unreplicated paternal pronuclei also became MeC-negative (Fig. 1d). This demethylation may be associated with transient hyperacetylation of histone H4 (ref. 7), because both replication and transcription are initiated earlier in the male pronucleus[8], which is less condensed.

At first metaphase, we observed two differentially methylated and spatially separated chromosome sets[9] (Fig. 1e). To exclude the possibility that differential MeC staining was due to changes in the accessibility of paternal DNA, we stained mouse embryos with anti-DNA antibody[10]: male and female pronuclei produced equally intense immunofluorescence (Fig. 1f–j). Two-cell embryos in phases G1 and G2 of the cell cycle were prepared at 22 and 32 hours. Most interphase nuclei displayed highly localized MeC staining (Fig. 1k,l), reflecting the compartmentalization of the two genomes, which may bring about the differential epigenetic reprogramming of the two genomes.

The amount of global methylation of the maternal genome was largely maintained from the early pronuclear to the two-cell stage, but four-cell embryos 45 hours after fertilization had a much lower MeC density over the maternal half of the nucleus (Fig. 1m). Interphase nuclei of 16- and 32-cell embryos had equivalently low methylation of paternal and maternal DNA (data not shown). Thus, in contrast to the very rapid and active demethylation of the paternal pronucleus, gradual demethylation of the maternal genome occurred passively during the second and third cleavage stages by a replication-dependent mechanism[9], which may involve the loss of maintenance methylase activity. The second polar body remained methylated throughout preimplantation development.

Our results provide a dramatic demonstration of the loss of DNA modification after fertilization. Active zygotic demethylation of the paternal genome has important implications for the understanding of genomic imprinting, X-chromosome inactivation, mammalian cloning and *in vitro* fertilization.

Wolfgang Mayer*†, Alain Niveleau‡, Jörn Walter*, Reinald Fundele*, Thomas Haaf*

**Max Planck Institute of Molecular Genetics, Ihnestrasse 73, 14195 Berlin, Germany*
e-mail: haaf@molgen.mpg.de
‡*Molecular and Structural Virology Unit, Université J. Fourier de Grenoble, 38706 La Tronche, France*
†*Deceased.*

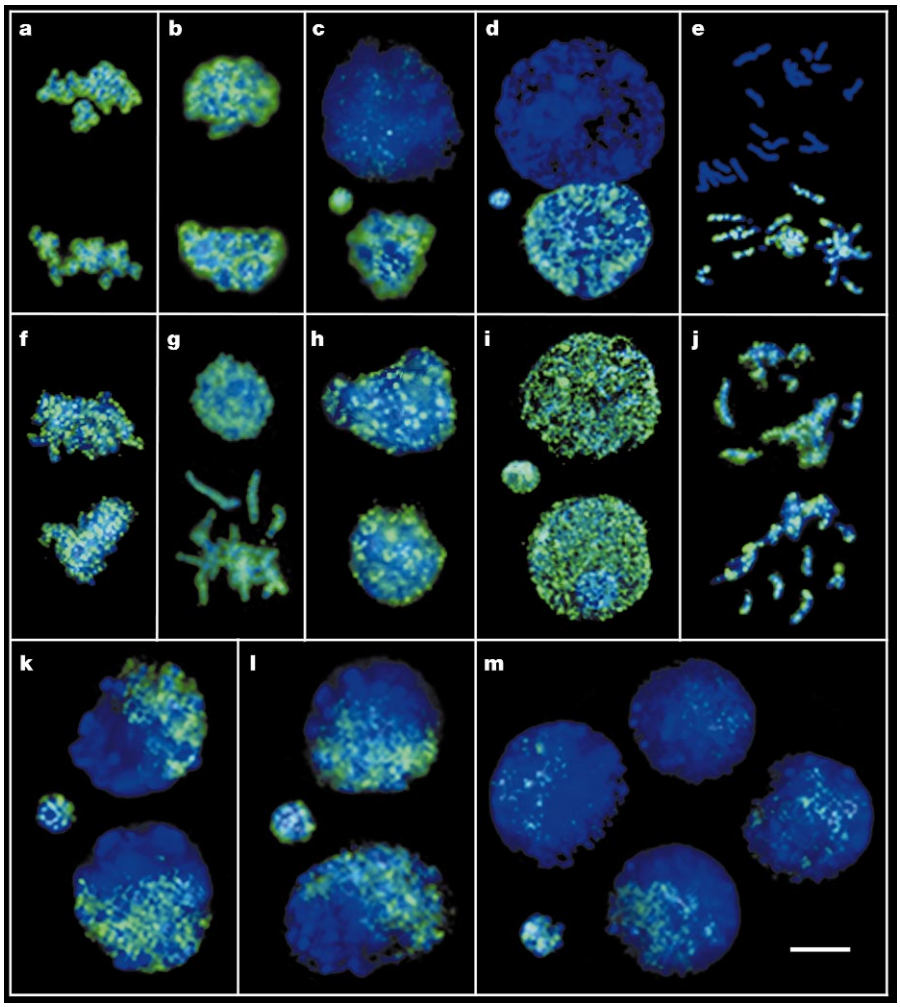

Figure 1 Differential demethylation of parental chromatin in the early mouse embryo. **a–e,** Anti-5-methylcytosine (MeC) immunofluorescence of mouse one-cell embryos. **a,** Zygote 3 h after fertilization with intense MeC labelling of both pronuclei (>10). Numbers in parentheses indicate the number of embryos analysed. **b,** Paternal and maternal pronuclei at 6 h (>10). **c,** Undermethylated paternal pronucleus at 8 h (>20). The smaller female pronucleus remains methylated. **d,** Aphidicolin-treated one-cell embryo displaying demethylation of the male pronucleus (>20). **e,** First metaphase (>5). **f–j,** Controls. Anti-DNA immunofluorescence of one-cell embryos demonstrates that both chromatin sets are accessible to antibody molecules. **f,** 3 h (>5). **g,** 6 h (>5). **h,** 8 h (>5). **i,** Aphidicolin treatment (>5). **j,** First metaphase (2). **k,l,** MeC staining of two-cell embryos at 22 h (>20) (**k**) and 32 h (>20) (**l**) shows that the paternal and maternal compartments have different methylation levels. **m,** Four-cell embryo at 45 h (>10). The MeC-staining intensity of the maternal half of the nucleus is weaker than in two-cell embryos. Scale bar, 10 μm.

1. Howlett, S. K. & Reik, W. *Development* **113,** 119–127 (1991).
2. Olek, A. & Walter, J. *Nature Genet.* **17,** 275–276 (1998).
3. Monk, M. *et al. Development* **99,** 371–382 (1987).
4. Yoder, J. A., Walsh, C. P. & Bestor, T. H. *Trends Genet.* **13,** 335–340 (1997).
5. Bird, A. P. *Nature* **321,** 209–213 (1986).
6. Howlett, S. K. *Roux's Arch. Dev. Biol.* **195,** 499–505 (1986).
7. Adenot, P. G. *et al. Development* **124,** 4615–4625 (1997).
8. Bouniol-Baly, C. *et al. Exp. Cell Res.* **236,** 201–211 (1997).
9. Rougier, N. *et al. Genes Dev.* **12,** 2108–2113 (1998).
10. Scheer, U. *Eur. J. Cell Biol.* **43,** 358–371 (1987).

Correction

Fluid 'rope trick' investigated

L. Mahadevan, W. S. Ryu, A. D. T. Samuel
Nature **392,** 140 (1998)

We wish to amend a small mistake in our calculations, although this does not affect the basic idea in our paper. As the longitudinal viscous stress σ in the filament scaled as $\sim \mu Ur/R^2$ varies linearly across the cross-section, the integrated stress resultant $\int \sigma dA$ vanishes. However, the net bending torque due to this viscous stress does not vanish and scales as $\int \sigma r dA \sim \mu Ur^4/R^2$. The force per unit volume on the fluid due to centripetal and Coriolis accelerations scales as $f \sim \rho\Omega^2 R$, so that the torque on the whirling filament in the vicinity of the coil scales as $fr^2R^2 \sim \rho\Omega^2 r^2 R^3$. Torque balance, together with the ancillary continuity relations, leads to a scaling law for the coiling frequency

$$\Omega \sim Q^{4/3} r^{-10/3} \nu^{-1/3} \quad (1)$$

which is slightly different from the result given in our paper, where an erroneous argument confuses the transverse and longitudinal timescales in the filament. Equation (1) can be derived directly using an analogy to the coiling of an elastic rope by simply replacing the elastic bending modulus Er^4 in ref. 1 with the 'viscous bending modulus' $\mu r^4 U/R$. A reconsideration of the experimental results leads to data collapse with a power law $\Omega/Q^{1.33} \sim r^{-3.45 \pm 0.10}$, in agreement with our argument.

1. Mahadevan, L. & Keller, J. B. *Proc. R. Soc. Lond. A* **452,** 1679–1694 (1996).